Onset of Fast Magnetic Reconnection

P. A. Cassak* and J. F. Drake

*Department of Physics and Institute for Research in Electronics and Applied Physics, University of Maryland,
College Park, Maryland 20742, USA*

M. A. Shay

Department of Physics and Astronomy, University of Delaware, Newark, Delaware 19716, USA

B. Eckhardt

*Fachbereich Physik, Phillipps-Universität Marburg, 35032 Marburg, Germany
Burgers Program, IREAP and IPST, University of Maryland, College Park, Maryland 20742, USA*

We demonstrate the existence of a new steady-state magnetic reconnection configuration which lies at the boundary of the basins of attraction between the Sweet-Parker and Hall reconnection configurations. The solution is linearly unstable to small perturbations and its identification required a novel iterative numerical technique. The eigenmodes of the unstable solution are localized near the X line, suggesting that the onset of fast reconnection in a weakly collisional plasma is initiated locally at the X line as opposed to remotely at the boundaries.

Magnetic reconnection is the process which converts magnetic energy into particle and flow energy in magnetic explosions in many space, astrophysical, and laboratory applications. Examples include solar flares, magnetic substorms, and sawtooth crashes in fusion devices. What causes these events to onset abruptly has long been an open question.

Much has been learned about why the energy conversion during magnetic reconnection takes place as fast as is observed. During (collisional) Sweet-Parker reconnection [1,2], the dissipation region is macroscopic in length [3–5], which throttles reconnection and renders it too slow to explain observed energy release rates [6]. During Hall reconnection [7,8], dispersive waves open the dissipation region into the microscopic Petschek open outflow configuration [9], producing reconnection fast enough to explain observed rates [7,10–12]. Signatures of Hall reconnection have been observed in the Earth's magnetosphere [13–17] and laboratory experiments [18,19].

A subject of ongoing debate in the literature concerns the dependence of Hall reconnection on the system size, which is related to the issue of the onset of Hall reconnection. Does the trigger of fast reconnection occur near the boundary and propagate inward to the X line or does it initiate near the X line and then propagate outward, making it insensitive to the boundaries? Some numerical results have found an independence of the steady-state reconnection rate on system size [11,20,21], suggesting the inside-out scenario. Others have found a dependence on system size [22–26], suggesting the outside-in scenario. In this Letter, we present evidence that the trigger is localized near the X line, suggesting that local physics rather than global dynamics controls fast reconnection.

It was recently shown that, in a system including both a resistivity η and the Hall effect, reconnection is bistable; i.e., both the Sweet-Parker and Hall reconnection solutions are independently valid for a wide range of resistivities [27]. For a system to have two stable steady-state solutions, there must also exist an unstable steady-state solution at the interface of the basins of attraction of the two stable solutions. In this Letter, we demonstrate the existence of the unstable steady-state reconnection configuration using numerical simulations of the Hall magnetohydrodynamic (Hall-MHD) equations. Finding unstable equilibria numerically is difficult because systems typically evolve away from unstable equilibria. We use a novel numerical technique recently developed for the onset of turbulence in fluid systems with shear flow [28,29]. After finding the unstable solution, we numerically exhibit its most unstable eigenmode, which is localized near the X line. This suggests that the transition from the macroscopic Sweet-Parker dissipation region to a Petschek-like open outflow configuration as fast reconnection onsets is initiated locally.

The numerical technique to find the unstable solution is iterative; beginning with two stable configurations ψ_f and ψ_s (or configurations evolving toward the two stable solutions), one takes weighted averages

$$\psi_\epsilon = \epsilon\psi_f + (1 - \epsilon)\psi_s, \qquad (1)$$

where ϵ is a constant weighting factor between 0 and 1, and ψ corresponds to all relevant dynamical variables, which for Hall-MHD are the plasma density n, the ion velocity $\mathbf{v}_i$, and the magnetic field $\mathbf{B}$. The subscripts f and s refer to fast and slow, respectively. By choosing various values of ϵ, one can bracket the unstable configuration; i.e., for one

value of ϵ the system returns to one stable state while for another it returns to the other, implying that the unstable configuration is between them. The process is repeated by taking weighted averages of the weighted averaged states, eventually converging to the unstable equilibrium.

The numerical simulations are performed using the massively parallel code F3D [21] to advance the equations of two-dimensional resistive Hall-MHD in a periodic domain of size $L_x \times L_y = 409.6d_i \times 204.8d_i$ with a cell size of $0.1d_i \times 0.1d_i$, where $d_i = c/\omega_{pi}$ is the ion skin depth and ω_{pi} is the ion plasma frequency. An electron mass of $m_e = m_i/25$ is used. Although this value is unrealistic, the electron mass only controls the thickness of the electron dissipation region. The domain is chosen large enough to be in the bistable regime while still sufficiently resolving the electron dynamics [27]. The resistivity and temperature are taken to be constant and uniform. There is no viscosity, but fourth order diffusion with coefficient 2×10^{-5} is used in all of the equations to damp noise at the grid scale. We normalize magnetic field strengths, densities, lengths, velocities, times, electric fields, and resistivities to characteristic asymptotic values of B_0, n_0, the ion skin depth $d_i = (m_i c^2/4\pi n_0 e^2)^{1/2}$, the Alfvén speed $c_{A0} = B_0/(4\pi m_i n_0)^{1/2}$, the ion cyclotron time $\Omega_{ci}^{-1} = (eB_0/m_i c)^{-1}$, $E_0 = c_{A0}B_0/c$, and $\eta_0 = 4\pi c_{A0}d_i/c^2$, respectively, where e and m_i are the ion charge and mass.

Convergence is expedited by constructing ψ_s and ψ_f using states in the process of making a transition to the Sweet-Parker and Hall solutions. Since the unstable solution is unique for a given resistivity, the specific initial states are of no consequence. We perturb a double Harris sheet equilibrium of initial width $2d_i$ and evolve the system with a resistivity $\eta = 0.015\eta_0$ until steady-state Sweet-Parker reconnection has been reached. Then, at a time of $t = 1098 \ \Omega_{ci}^{-1}$, we abruptly lower the resistivity to $\eta = 0.007\eta_0$ and the system makes a transition to Hall reconnection. In Fig. 1(a), the current sheet thickness δ (measured as the half width at half maximum of the out of plane current density J_z) during the transition is shown as a function of time by the solid line. The thickness of the steady-state Sweet-Parker layer is $1.22d_i$. It is $d_e \simeq 0.2d_i$ during Hall reconnection. During the transition (at $t = 1278 \ \Omega_{ci}^{-1}$), we abruptly return η to $0.015\eta_0$. The upper dashed line indicates that the system begins to revert back to Sweet-Parker reconnection. However, when η is returned to $0.015\eta_0$ later during the transition (at $t = 1428 \ \Omega_{ci}^{-1}$), the system continues to the Hall configuration, as shown in the lower dashed line. We take the states marked by the boxes in Fig. 1(a) as our initial states: ψ_s at $t = 1510.5 \ \Omega_{ci}^{-1}$ on the upper dashed line (with $\delta = 0.78d_i$) and ψ_f at $t = 1443 \ \Omega_{ci}^{-1}$ on the lower dashed line (with $\delta = 0.43d_i$).

Results of the iteration procedure are plotted in Fig. 1(b). The upper and lower solid lines show δ as a function of time for the first iteration with $\epsilon = 0.7$ and 0.9, respectively. After a transient time where δ decreases, it increases
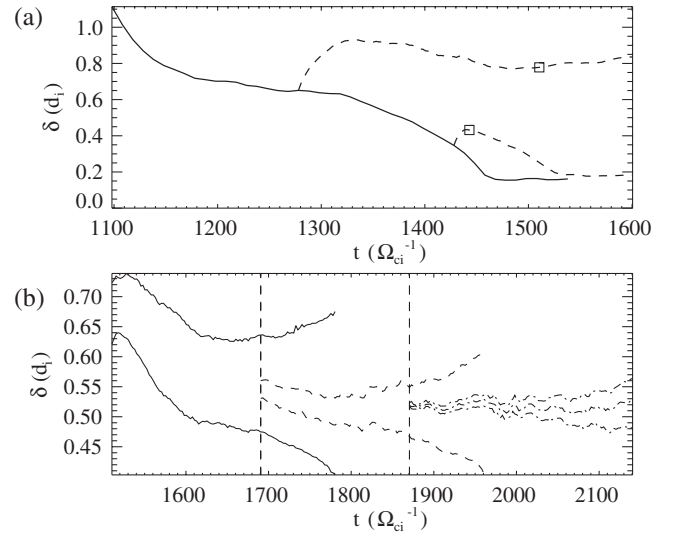
FIG. 1. (a) Current sheet thickness δ as a function of time for the procedure to create initial states ψ_f and ψ_s. Convergence is expedited by using the states denoted by the boxes as initial conditions. (b) Results of the iteration procedure for finding the unstable equilibrium. The first, second, and third iterations are shown as the solid, dashed, and dot-dashed lines, respectively. The vertical lines mark the times which define the initial state for the following iteration.

back toward the Sweet-Parker solution for $\epsilon = 0.7$ and decreases toward the Hall solution for $\epsilon = 0.9$. The second iteration is initiated using the states on the two solid lines at $t = 1690.5 \ \Omega_{ci}^{-1}$. The upper and lower dashed lines are a result of using $\epsilon = 0.4$ and 0.6, respectively, which after an initial transient, evolve toward the two stable configurations. The third iteration is initiated using the states on the two dashed lines at $t = 1870.5 \ \Omega_{ci}^{-1}$. The upper and lower dot-dashed lines are the results of using $\epsilon = 0.6$ and 0.7, respectively. One can see that the iteration procedure is converging.

In principle, this iteration procedure could continue indefinitely. However, since our periodic domain only has a finite amount of magnetic flux available to be reconnected, we finish by taking an intermediate value of $\epsilon = 0.65$ in the third iteration, plotted as the middle dot-dashed line starting at $t = 1870.5 \ \Omega_{ci}^{-1}$. The system stays at a nearly constant δ for an exceedingly long time (about $200 \ \Omega_{ci}^{-1}$, or 7 Alfvén wave transit times down the sheet). During this time, the configuration is essentially in the unstable equilibrium.

What are the properties of the unstable steady-state reconnection solution at this η? The out of plane current density J_z of the unstable solution is shown in Fig. 2(b) at $t = 2055.5 \ \Omega_{ci}^{-1}$. For comparison, the steady-state Hall and Sweet-Parker solutions are shown in Figs. 2(a) and 2(c), respectively; only a fraction of the whole domain is plotted. As expected, the properties of the unstable solution are intermediate between the Sweet-Parker and Hall solutions, with the downstream current sheet of the unstable
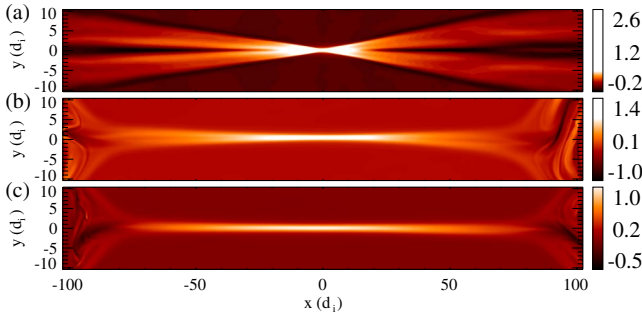
FIG. 2 (color online). Profile of the out of plane current density J_z for the three steady-state magnetic reconnection solutions: (a) Hall, (b) the unstable solution, (c) Sweet-Parker.

solution opening wider than the Sweet-Parker current sheet, but not as wide as the Hall sheet.

The half thickness of the dissipation region is $\delta \simeq 0.51 d_i$, clearly distinct from the Sweet-Parker and Hall values. The length of the current sheet, measured as the half width at half maximum of the out of plane current density J_z in the outflow direction, is $L \simeq 30 d_i$, which is again intermediate between the Sweet-Parker and Hall values. The steady-state reconnection rate is $E \simeq 0.017 E_0$. For comparison, the Sweet-Parker and Hall reconnection rates are about $0.014 E_0$ and $0.06 E_0$, respectively.

What are the properties of the unstable solution for other resistivities? In an upcoming paper, we present a model of reconnection dynamics using saddle-node bifurcations, which makes predictions about the unstable equilibrium. In particular, δ counterintuitively decreases with increasing η. Further, a scaling analysis predicts that E scales linearly with η.

The difference between the upper or lower dot-dashed line of Fig. 1(b) and the equilibrium state (the middle dot-dashed line) can be treated as a small perturbation to the equilibrium solution. The difference in δ between the unstable state and the state diverging toward the Hall and Sweet-Parker solutions (the lower and upper dot-dashed lines) are plotted as a function of time as the thick solid and dashed lines in Fig. 3. The fact that the data fall nicely on a straight line indicates that the system is in a linear regime with one mode dominating the evolution and that the eigenvalue is purely real. The slope of the line gives a growth rate of $\gamma \sim 0.008 \, \Omega_{ci}$ (corresponding to a growth time of $\tau = 1/\gamma \sim 125 \, \Omega_{ci}^{-1}$). For comparison, the Alfvén wave transit time down the current sheet and the diffusive time across the current sheet are $\tau_{Tr} \sim 30 \, \Omega_{ci}^{-1}$. The diffusive time along the sheet is $\tau_r \sim 6 \times 10^4 \, \Omega_{ci}^{-1}$.

The physical structure of the most unstable eigenmode is calculated by taking the difference of the relevant dynamical variables (n, $\mathbf{v}_i$, and $\mathbf{B}$) between the system diverging toward the Hall solution and the equilibrium solution [the lower and middle dot-dashed lines of Fig. 1(b), respectively]. Figure 4 shows the eigenmodes of the derived quantities $J_z = (c/4\pi)\hat{\mathbf{z}} \cdot \nabla \times \mathbf{B}$, the out of plane current density, and $\omega_z = \hat{\mathbf{z}} \cdot \nabla \times \mathbf{v}_i$, the out of plane component
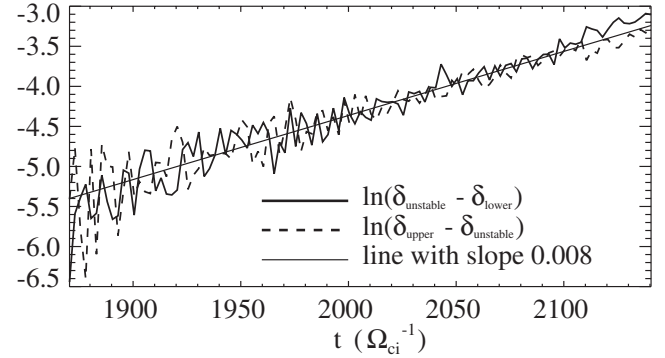
FIG. 3. Natural logarithm of the difference in δ between the lower (upper) dot-dashed line of Fig. 1(b) and the middle dot-dashed line plotted as a function of time t as the solid (dashed) line. The slope of the line, about $0.008 \, \Omega_{ci}$, gives the eigenvalue (growth rate) for the most unstable eigenmode to the unstable equilibrium.

of the ion vorticity, zoomed in around the X line at $t = 2045.5 \, \Omega_{ci}^{-1}$.

The eigenmodes are seen to initiate the transition from the unstable to the Hall solution. Specifically, the J_z eigenmode is consistent with the opening out of the magnetic field in the downstream region as the Petschek open outflow configuration is set up. Further, the ω_z eigenmode is such that the ion inflow speed increases, thereby increasing the reconnection rate as the transition to Hall reconnection begins.

Both eigenmodes have their magnitudes peaked in a localized region near the X line of the unstable equilibrium configuration. The localization of the vorticity again reveals that the dissipation region is opening out into the Petschek geometry. The ω_z structure is consistent with vertical flow away from the neutral line about $15 \, d_i$ downstream of the X line. This flow serves to open the outflow region.

Since the structure of the eigenmodes grows exponentially with time in the linear growth phase, the first signal of fast reconnection will occur locally near the X line where the eigenmodes are peaked. This strongly supports the hypothesis that the onset of Hall reconnection is initiated
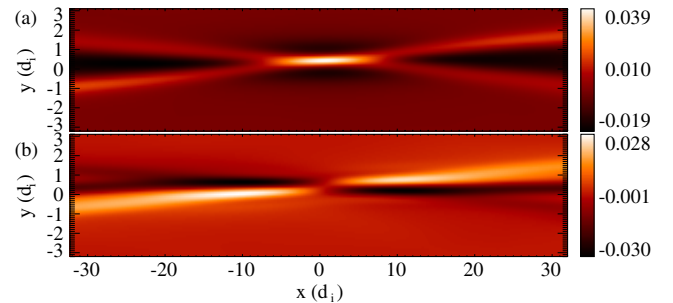
FIG. 4 (color online). The structure of the (a) out of plane current density J_z and (b) the out of plane ion vorticity ω_z of the most unstable eigenmode of the unstable equilibrium.

at the X line due to local physics as opposed to being initiated due to physics at the boundaries.

The local structure in J_z and ω_z has a length scale in the outflow direction of about 10–$15d_i$, which is the same as the intrinsic length scale of the ion dissipation region during (fully nonlinear) Hall reconnection. In particular, the structure of the ion vorticity eigenmode is quite similar to the ion vorticity during fully nonlinear Hall reconnection. This suggests that the eigenmode of the unstable equilibrium contains the salient physics which determines the structure of the ion dissipation region during Hall reconnection.

We emphasize that the microscopic ($\sim 10d_i$) structure seen in the eigenmode evolves from the unstable equilibrium which is mesoscopic, with structure on scales of $\sim 30d_i$. No numerical techniques are used to introduce microscopic structure into the unstable equilibrium: the microscopic structure is generated self-consistently.

The present results are consistent with the interpretation of Hall reconnection being mediated by whistler physics [30]. In this model, onset occurs when the dissipation region becomes thinner than d_i. At this length scale, the standing waves generating the outflow jets change from Alfvén waves to whistler waves [30]. The electron outflow speed associated with whistler waves increases, but only close to the X line where the length scales are the smallest. The increased electron outflow diverges transverse to the outflow direction as shown in Fig. 4, opening up the outflow jet into the Petschek configuration characteristic of fast reconnection [8].

The model presented here is limited by being only two-dimensional with a constant and uniform resistivity and temperature. Also, these simulations do not contain an initial out of plane (guide) magnetic field. It was recently shown [31] that reconnection with a strong guide field is also bistable, so results similar to those presented here should be obtainable for reconnection with a guide field.

Lastly, it should be emphasized that the collisionality of the system is playing a key role in the present result. In a purely collisionless plasma, the present result would only be expected to carry over if there were an effective turbulent resistivity which supported a Sweet-Parker type dissipation region thicker then d_i.

---

*Present address: Department of Physics and Astronomy, 217 Sharp Laboratory, University of Delaware, Newark, DE 19716, USA.

[1] P. A. Sweet, in *Electromagnetic Phenomena in Cosmical Physics*, edited by B. Lehnert (Cambridge University Press, Cambridge, England, 1958), p. 123.

[2] E. N. Parker, J. Geophys. Res. **62**, 509 (1957).

[3] D. Biskamp, Phys. Fluids **29**, 1520 (1986).

[4] D. A. Uzdensky and R. M. Kulsrud, Phys. Plasmas **7**, 4018 (2000).

[5] B. D. Jemella, J. F. Drake, and M. A. Shay, Phys. Plasmas **11**, 5668 (2004).

[6] E. N. Parker, Astrophys. J. **8**, 177 (1963).

[7] J. Birn, J. F. Drake, M. A. Shay, B. N. Rogers, R. E. Denton, M. Hesse, M. Kuznetsova, Z. W. Ma, A. Bhattacharjee, and A. Otto *et al.*, J. Geophys. Res. **106**, 3715 (2001).

[8] B. N. Rogers, R. E. Denton, J. F. Drake, and M. A. Shay, Phys. Rev. Lett. **87**, 195004 (2001).

[9] H. E. Petschek, in *AAS/NASA Symposium on the Physics of Solar Flares*, edited by W. N. Ness (NASA, Washington, DC, 1964), p. 425.

[10] A. Y. Aydemir, Phys. Fluids B **4**, 3469 (1992).

[11] M. A. Shay, J. F. Drake, B. N. Rogers, and R. E. Denton, Geophys. Res. Lett. **26**, 2163 (1999).

[12] A. Bhattacharjee, Z. W. Ma, and X. Wang, J. Geophys. Res. **104**, 14 543 (1999).

[13] M. Øieroset, T. D. Phan, M. Fujimoto, R. P. Lin, and R. P. Lepping, Nature (London) **412**, 414 (2001).

[14] T. Nagai, I. Shinohara, M. Fujimoto, M. Hoshino, Y. Saito, S. Machida, and T. Mukai, J. Geophys. Res. **106**, 25 929 (2001).

[15] F. Mozer, S. D. Bale, and T. D. Phan, Phys. Rev. Lett. **89**, 015002 (2002).

[16] A. Runov, R. Nakamura, W. Baumjohann, R. A. Treumann, T. L. Zhang, M. Volwerk, Z. Vörös, A. Balogh, K.-H. Glabmeier, and B. Klecker *et al.*, Geophys. Res. Lett. **30**, 1579 (2003).

[17] A. L. Borg, M. Øieroset, T. D. Phan, F. S. Mozer, A. Pedersen, C. Mouikis, J. P. McFadden, C. Twitty, A. Balogh, and H. Rème, Geophys. Res. Lett. **32**, L19105 (2005).

[18] Y. Ren, M. Yamada, S. Gerhardt, H. Ji, R. Kulsrud, and A. Kuritsyn, Phys. Rev. Lett. **95**, 055003 (2005).

[19] C. D. Cothran, M. Landreman, M. R. Brown, and W. H. Matthaeus, Geophys. Res. Lett. **32**, L03105 (2005).

[20] J. D. Huba and L. I. Rudakov, Phys. Rev. Lett. **93**, 175003 (2004).

[21] M. A. Shay, J. F. Drake, M. Swisdak, and B. N. Rogers, Phys. Plasmas **11**, 2199 (2004).

[22] D. Grasso, F. Pegoraro, F. Porcelli, and F. Califano, Plasma Phys. Controlled Fusion **41**, 1497 (1999).

[23] X. Wang, A. Bhattacharjee, and Z. W. Ma, Phys. Rev. Lett. **87**, 265003 (2001).

[24] F. Porcelli, D. Borgogno, F. Califano, D. Grasso, M. Ottaviani, and F. Pegoraro, Plasma Phys. Controlled Fusion **44**, B389 (2002).

[25] R. Fitzpatrick, Phys. Plasmas **11**, 937 (2004).

[26] A. Bhattacharjee, K. Germaschewski, and C. S. Ng, Phys. Plasmas **12**, 042305 (2005).

[27] P. A. Cassak, M. A. Shay, and J. F. Drake, Phys. Rev. Lett. **95**, 235002 (2005).

[28] J. D. Skufca, J. A. Yorke, and B. Eckhardt, Phys. Rev. Lett. **96**, 174101 (2006).

[29] T. M. Schneider, B. Eckhardt, and J. A. Yorke (to be published).

[30] M. E. Mandt, R. E. Denton, and J. F. Drake, Geophys. Res. Lett. **21**, 73 (1994).

[31] P. A. Cassak, J. F. Drake, and M. A. Shay, Phys. Plasmas **14**, 054502 (2007).